Molecular origin of photovoltaic performance in donor-*block*-acceptor all-conjugated block copolymers.

Kendall A. Smith,[1] Yen-Hao Lin,[1] Jorge W. Mok,[1] Kevin G. Yager,[2] Joeseph Strzalka,[3] Wanyi Nie,[4] Aditya Mohite,[4] and Rafael Verduzco[1].*

[1]Rice University, 6100 Main St., Houston, TX, USA, 77005

[2]Center for Functional Nanomaterials, Brookhaven National Laboratory, Upton, New York 11973

[3]X-ray Science Division, Argonne National Laboratory, Argonne, Illinois 60439

[4]Materials Physics and Applications (MPA) Division, Mail Stop: K771, Los Alamos National Laboratory (LANL), Los Alamos, New Mexico 87544

KEYWORDS. P3HT, poly(3-hexylthiophene), PFTBT, PF8TBT, all-conjugated, block copolymer, all-polymer, self-assembly, organic photovoltaics, organic solar cells.

ABSTRACT.

All-conjugated block copolymers may be an effective route to self-assembled photovoltaic devices, but we lack basic information on the relationship between molecular characteristics and photovoltaic performance. Here, we synthesize a library of poly(3-hexylthiophene) (P3HT) *block* poly((9,9-dialkylfluorene)-2,7-diyl-alt-[4,7-bis(alkylthiophen-5-yl)-2,1,3-benzothiadiazole]-2□,2□-diyl) (PFTBT) donor-*block*-acceptor all-conjugated block copolymers and carry out a comprehensive study of processing conditions, crystallinity, domain sizes, and side-chain structure on photovoltaic device performance. We find that all block copolymers studied exhibit an out-of-plane crystal orientation after deposition, and on thermal annealing at high temperatures the crystal orientation flips to an in-plane orientation. By varying processing conditions on polymer photovoltaic devices, we show that the crystal orientation has only a modest effect (15-20%) on photovoltaic performance. The addition of side-chains to the PFTBT block is found to decrease photovoltaic power conversion efficiencies by at least an order of magnitude. Through grazing-incidence X-ray measurements we find that the addition of side-chains to the PFTBT acceptor block results in weak segregation and small (< 10 nm) block copolymer self-assembled donor and acceptor domains. This work is the most comprehensive to date on all-conjugated block copolymer systems and suggests that photovoltaic performance of block copolymers depends strongly on the miscibility of donor and acceptor blocks, which impacts donor and acceptor domain sizes and purity. Strategies for improving the device performance of block copolymer photovoltaics should seek to increase segregation between donor and acceptor polymer domains.

Introduction

Bulk heterojunction organic photovoltaic devices (OPVs) have the potential to be a low cost method of collecting solar energy and are attractive due to their ease of processing.[1–4] State-of-the-art OPVs are prepared by blending a low bandgap polymer with a fullerene derivative, which acts as the electron acceptor.[5] Donor and acceptor polymers can also be blended to make a bulk heterojunction photovoltaic device. However, the final morphology of bulk heterojunction blends is dictated by non-equilibrium phase separation, potentially resulting in large-scale phase separation and poor control over morphology.

An alternative approach involves the use of materials that can self-assemble to form distinct donor and acceptor domains.[6–10] However, there are only a few reports of all-conjugated block copolymer systems with energy levels capable of producing workable devices.[11–14] Recently, we reported on the block copolymer poly(3-hexylthiophene)-*block*-poly((9,9-dioctylfluorene)-2,7-diyl-alt-[4,7-bis(thiophen-5-yl)-2,1,3-benzothiadiazole]-2□,2□-diyl) (P3HT-*b*-PF8TBT) which achieved a performance of 3%, significantly above that of the corresponding homopolymer blend device[15–17]. This block copolymer system enables us to systematically investigate the relationship between molecular structure, processing history, morphology, and photovoltaic performance in all-conjugated block copolymer systems.

In just the past several years, significant progress has been made in all-polymer solar cells and reported efficiencies of all-polymer blend devices.[18–23] Particularly relevant for our work, a similar polymer blend system has been shown to have efficiencies as high as 2.7% with very high molecular weight acceptor polymer.[24] It is worth noting that thus far many polymers selected for use in block copolymer devices have been based on polymers that have performed reasonably well in polymer blends, and in many cases the performance of block copolymers is

inferior to that of corresponding homopolymer blends.[14,25,26] Homopolymers that perform well in blends generally do so because they have inherently limited phase separation[27,28], but a better approach in block copolymer systems may be to utilize polymers that have stronger segregation in order to obtain higher purity domains. An understanding of the characteristics of all-conjugated block copolymer that contribute to enhanced photovoltaic properties is needed to advance work with these materials. This includes optimal domain size, processing conditions, crystal orientation, side-chain structure, and annealing history.

In this work, we explore the influence of side-chain structure and processing conditions on morphology and photovoltaic performance of all-conjugated block copolymers. Altering side chains affects solubility and packing of the PFTBT block, and modifying the conjugated polymer side-chains potentially provides a way to tune the P3HT crystal orientation, the degree of phase separation in the block copolymer, and the photovoltaic performance of the material. We assess crystallization, crystalline orientation, and microphase segregation in a series of block copolymers of P3HT-*b*-PFTBT where the alkyl side chains of the PFTBT are systematically varied. We also correlate morphological studies using grazing incidence small/wide angle X-ray scattering (GISAXS/GIWAXS) with device performance to understand the molecular origin of photovoltaic performance in all-conjugated block copolymer systems. We find that the attachment of side chains to the PFTBT block worsens solar cell performance, which we attribute to increased miscibility between the blocks and reduced donor and acceptor domain sizes. We find that the crystal orientation has a strong dependence on processing history, in particular the annealing temperature, and find that the orientation of the P3HT crystals only has a modest effect on photovoltaic performance. These results suggest that future work aimed at

improving block copolymer OPV device should focus on increasing domain sizes and segregation strength between polymer blocks.

Discussion

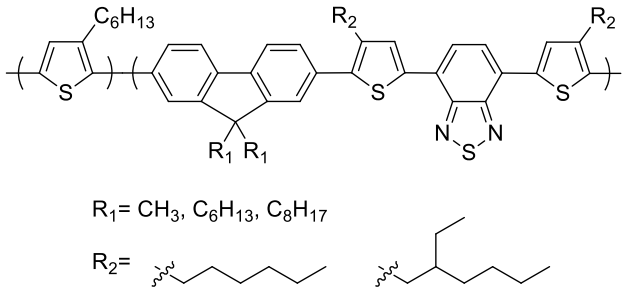

Figure 1: Structures of P3HT-*b*-PFTBT block copolymers studied. P3HT is the donor block and PFTBT with various side chains as the acceptor block. Side chains on the fluorene unit (R_1) were methyl, hexyl, and octyl and are denoted as F1, F6, and F8, respectively. Hexyl, ethyl-hexyl and hydrogen on the dithiophene-benzothiadiazole unit (R_2), are denoted HTBT, EHTBT and TBT, respectively.

In this work, we synthesized and studied block copolymers consisting of P3HT-*b*-PFTBT where the side-chains on the PFTBT block are systematically varied as shown in Figure 1. The side chains chosen here were selected to provide a range of different alkyl side chains and improve solubility of the final block copolymer.[29] The goal was to investigate the impact on the morphology and performance of these materials while not significantly altering the optoelectronic properties of the backbone. Synthesis of these block copolymers was performed by a sequential Grignard Metathesis (GRIM) polymerization followed by an end-capping Suzuki reaction approach that has been reported previously.[15,30–32] Block copolymers were then purified by washing with acetone and boiling hexanes to remove PFTBT oligomers. A total of 30 different block copolymer samples were synthesized differing in the molecular weight of the

P3HT block, the molecular weight of the PFTBT block, and the side-chains attached to the PFTBT block. Homopolymers of P3HT and each of the PFTBT blocks were also made and full characteristics of homopolymers and block copolymers are provided in Supporting Information (Tables S1 & S2) along with ^{1}H NMR data for each type of block copolymer (Figure S1). Thin film absorbance measurements for each of the PFTBT acceptor blocks are shown in the Supporting Information Figure S2 and show that the various side-chains do not have a significant impact on polymer absorbance.

Extensive evaluation of the purity of these samples was performed to quantify the amounts of homopolymer impurities. Our analysis also provides an estimate of the relative amounts of P3HT-*b*-PFTBT diblock copolymer and P3HT-*b*-PFTBT-*b*-P3HT triblock copolymer in each sample. In brief, to perform this analysis we used size exclusion chromatography with ultraviolet/visible (UV/Vis) detection for the relative mass of each polymer block at each elution time. Additionally, ^{1}H NMR data provides an average composition for each block copolymer sample. We then use a standard optimization method to solve simultaneously for molecular weight distributions of PFTBT homopolymer, PFTBT in diblock and triblock block copolymers, the relative mass fractions of block copolymers and homopolymers, and the molecular weight as a function of elution time. The molecular weight of a P3HT homopolymer is fixed to the value determined by multi-angle light scattering. Full details of the analysis are provided in Supporting Information ("Determination of Block Copolymer Purity", Figures S3 & S4) along with characteristics of all block copolymers synthesized for this work (Table S2). In general, we find that all samples are majority block copolymer with a mixture of diblock P3HT-*b*-PFTBT and triblock P3HT-*b*-PFTBT-*b*-P3HT. Such detailed analysis is not typically carried out on conjugated block copolymer samples, although one recent study found similar degrees of

polymeric impurities in conjugated block copolymers prepared through polycondensation reactions.[29]

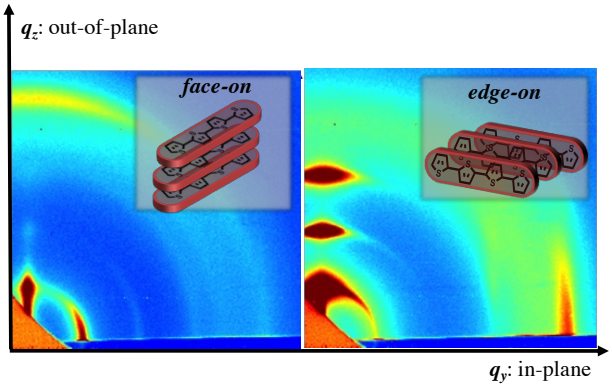

Figure 2: Schematics for face-on and edge-on orientation of P3HT crystallites and corresponding 2-D GIWAXS. A strong π–π stacking peak is prominent in the out-of-plane direction for the face-on orientation, while edge-on crystallites exhibit only alkyl stacking peaks in the out-of-plane direction.

First, we focus our attention on the crystal orientation and the potential effect on performance. A notable feature of the all-conjugated block copolymer system we reported previously[15] was an orientation of the π–π stacking direction in the out-of-plane direction, also known as a face-on orientation as shown in Figure 2. Regioregular P3HT homopolymer films have been previously analyzed by GIWAXS and show a preference for edge-on orientation with the π–π stacking direction in-plane.[33,34] The orientation of the π–π stacking direction has a significant impact on the electronic properties of conjugated polymer films, and here we seek to characterize the crystal orientation the series of P3HT-*b*-PFTBT block copolymers as a function of side-chain composition and processing history and understand the resulting impact on photovoltaic performance.

Films were either thermally annealed at 165 °C or 230 °C or solvent annealed with chloroform at room-temperature, and films were cast from either room temperature or refluxing solvent. Crystal melting temperatures for all block copolymer samples are provided in the Supporting Information Table S4. All block copolymer samples exhibit crystal melting temperatures above 165 °C and below or near 230 °C. GIWAXS measurements show a strong dependence of crystal orientation on processing history (Figure 3). For our analysis, we are assuming that polymers are oriented in a predominantly edge-on (π stacking in-plane, alkyl stacking out-of-plane), face-on (π stacking out-of-plane, alkyl stacking in-plane), or isotropic orientation and neglect the potential for end-on configuration (π stacking and alkyl stacking in-plane and polymer ends out-of-plane).[35,36] In order to assess the amount of material that has edge-on versus face-on, the orientational anisotropy of the P3HT alkyl stacking peak at $q = 0.38$ Å^{-1} was analyzed. This peak was used for analysis in favor of the π stacking peak at 1.6 Å^{-1} since it has a larger signal-to-noise ratio. A detailed discussion of how this analysis was performed is included in Supporting Information (Figure S5).

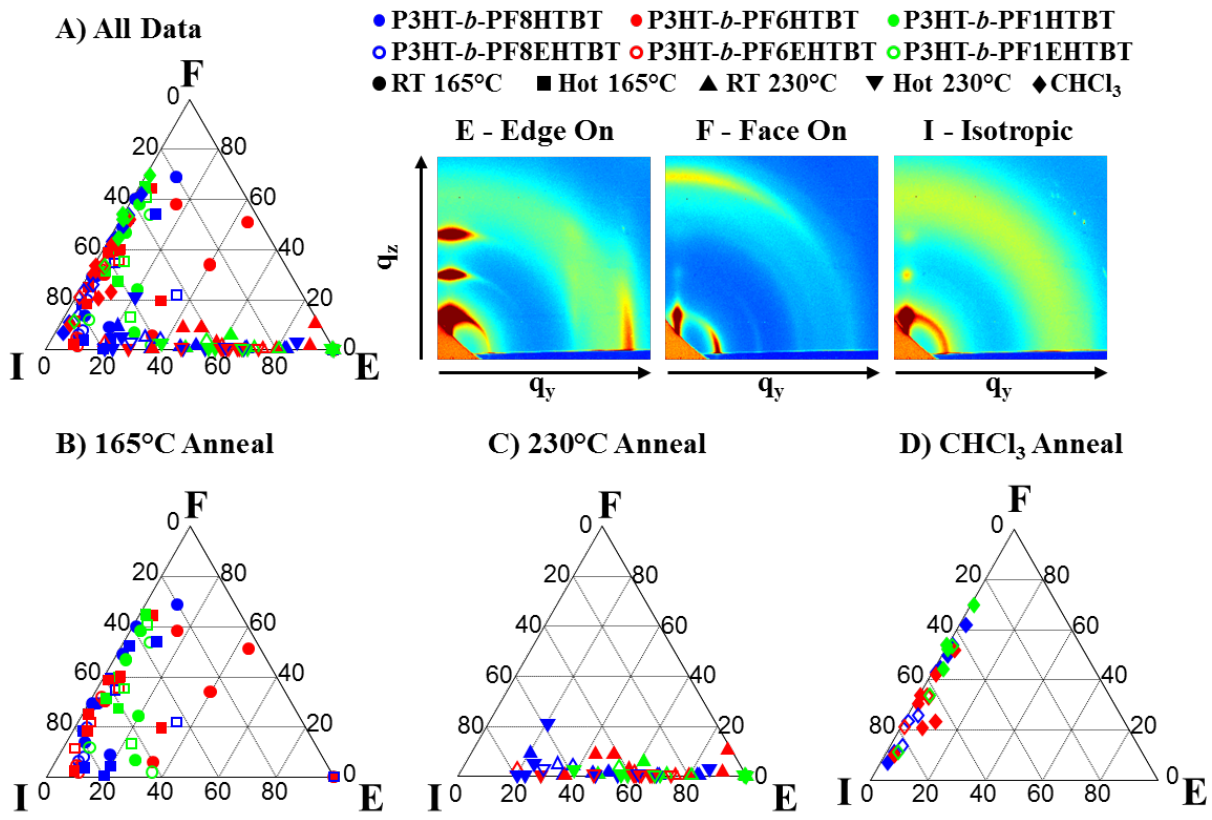

Figure 3: Ternary plots of crystal orientation for polymer films analyzed by GIWAXS. Polymers were processed from room temperature solvent and annealed at 165 °C (●) or 230 °C (▲) or spin-cast from refluxing (Hot) solvent and annealed at 165 °C (■) or 230 °C (▼). Polymers processed from room temperature solvent were also solvent annealed with room temperature chloroform (♦). Alkyl chain lengths of 8, 6, and 1 on the fluorene unit of PFTBT are indicated by blue, red, and green respectively. Side chains on the thiophene units of PFTBT are indicated by closed symbols (hexyl) and open symbols (ethyl-hexyl). GIWAXS images of predominantly edge-on (E), face-on (F), and isotropic (I) distributions are included for reference. (A) Shows all the data in a single ternary plot, while (B), (C), and (D) show 165°C, 230°C and solvent annealed cases respectively.

Figure 3 shows a ternary plot summarizing the resulting distribution of P3HT crystal orientation as a function of processing conditions and side chain architecture. Figure 3A shows all the data where it can be seen that most samples show orientations that are split between the isotropic and either a face-on or edge-on orientation. As can readily be seen by comparing Figure 3B with Figure 3C, annealing at 165 °C (below the melting temperature of P3HT in the block copolymer) results in a crystal orientation with face-on character while annealing at 230 °C (above the melting temperature of P3HT in the block copolymer) results in an edge-on crystal orientation. This is also observed when plotting the data as a function of the difference between the annealing temperature and melting point for each block copolymer as shown in the Supporting Information Figure S6. The crystal orientation is preferentially edge-on when annealing above the crystal melting temperature and face-on when annealing below the crystal melting temperature. In the case of solvent annealing at room temperature, as shown in Figure 3D, we see very little of the edge-on orientation. The solvent annealed samples generally have less crystallinity compared to the thermally annealed samples as indicated by lower intensity peaks in X-ray scattering. In general, we find that the P3HT orientation is primarily driven by the annealing temperature. The other factors investigated, such as side chain length on the PFTBT unit and casting from room temperature or refluxing solvent, do not have a dramatic effect on the final orientation.

These measurements show that crystal orientation, and as a result electronic properties, can be tuned by varying processing conditions, specifically the post-deposition annealing temperature. To observe the structure of the polymer films evolve during the annealing process, several polymers were analyzed by temperature-dependent, *in situ* GIWAXS measurements. Selected samples were subjected to heating cycles reaching 165 °C or 220 °C (maximum temperature

obtainable using beamline equipment) and GIWAXS images were taken roughly every 5 °C with the sample periodically moved slightly during measurements to avoid excessive beam damage. A sampling of different polymers was selected for detailed study: P3HT9-*b*-PF8TBT, P3HT2-*b*-PF8HTBT3, and P3HT7-*b*-PF1EHTBT1 (Table S2). These were selected to represent a range of the different side chains for the PFTBT block ranging from eight to one carbon on the fluorene and ethyl-hexyl, hexyl, and hydrogen for side-chains on the thiophene rings. The key observations of the *in situ* GIWAXS measurements are summarized in Figure 4. In general, films cooled from below the melting point show a face-on orientation indicated by the peak near 1.6 $Å^{-1}$ along q_z and at 0.38, 0.76, and 1.14 $Å^{-1}$ along q_y. The peaks associated with alkyl and π stacking completely disappear when heated above the melting point (Figure 4B), and the usual in-plane π stacking and out-of-plane alkyl stacking associated with the edge-on P3HT orientation are observed upon cooling from 220°C (Figure 4C). Note that in 4C, peaks initially oriented along q_z in Figure 4A are now oriented along q_y. A more detailed discussion of the *in situ* GIWAXS measurements are provided in the Supporting Information, including the differential scanning calorimetry (DSC) data for these polymers (Figure S7), key transitions in the GIWAXS measurements (Figure S8), and video files of the *in situ* GIWAXS measurements.

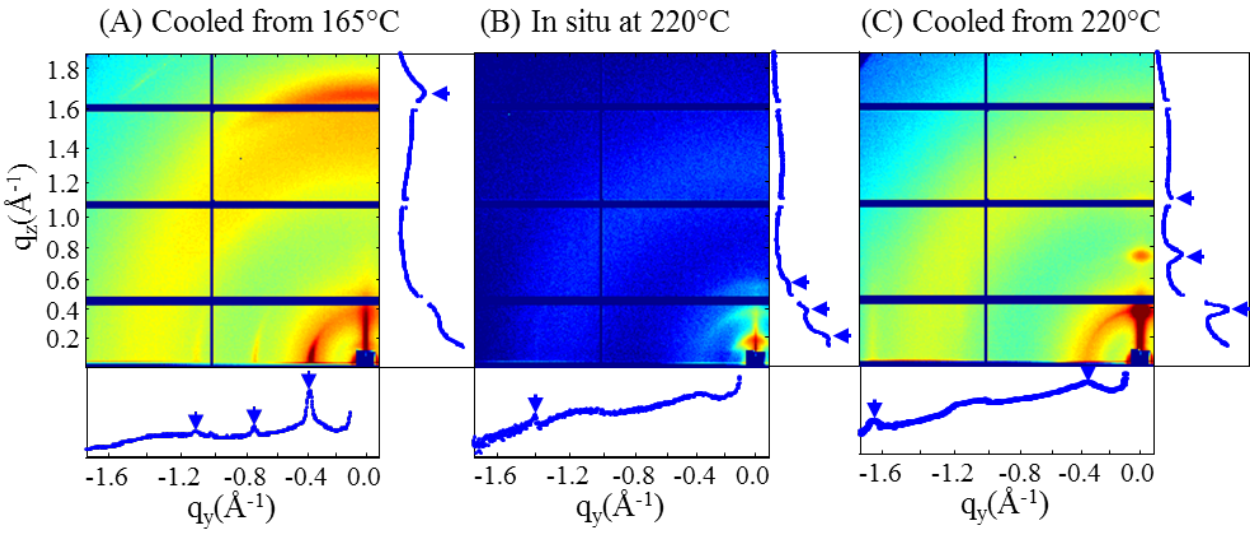

Figure 4: Summary of GIWAXS results of *in situ* measurements of P3HT-*b*-PF8HTBT films cooled from 165 °C (A), *in situ* at 220 °C (B) and cooled from 220 °C (C) showing the change in orientation of P3HT after annealing above the melting point. Linecuts in q_y and q_z are included adjacent to each GIWAXS image with peaks denoted by arrows.

The physical picture for why the P3HT crystallites have a face-on orientation is still unclear, but with the available data we can outline a sequence that explains the observations (Figure 5). Prior work on X-ray reflectivity of PF8TBT/P3HT homopolymer blend films revealed that the PFTBT homopolymer preferred to segregate to the substrate interface.[36,37] We hypothesize that preferential segregation of the PFTBT block to the substrate may reduce or eliminate the preference of P3HT alkyl stacking normal to the surface. Additionally, although phase separation may be weak, we expect our block copolymer is separating into roughly vertical nanodomains that may be helpful in producing films that have a face-on configuration.[36] *In situ* measurements have revealed a lamellar structure assignable to PFTBT in the block copolymer that has large domain spacing associated with it. This may lead to some geometric constraint that favors a face-on orientation of P3HT to accommodate the large lattice of the PFTBT block (as depicted in

Figure 5A). Whatever the cause of the initial face-on orientation of P3HT, this configuration is clearly robust until the block copolymer film is heated above its melting point (Figure 5B). Here, P3HT in the melt is able to order itself relative to the substrate and, as the film is cooled, the normal P3HT alkyl stacking pattern is observed (Figure 5C). It is noted that this comes at the cost of the ordering of the PFTBT polymer and elimination of the corresponding peaks in GIWAXS.

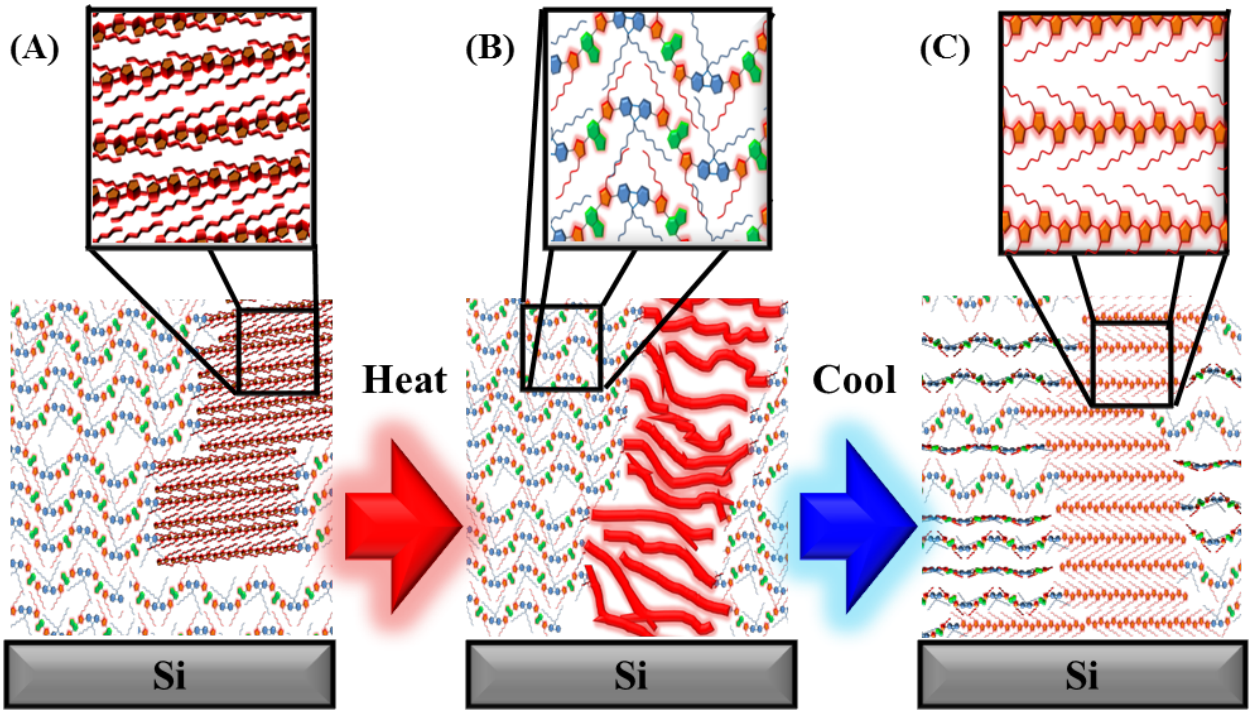

Figure 5: Schematic of evolution of block copolymer film after casting. (A) shows as cast film with P3HT face-on. Upon heating above the melting point (B) the P3HT crystals melt and a lamellar structure (PFTBT) can be observed. After cooling (C), the P3HT crystals reform with an edge on orientation and disrupt the structure of PFTBT.

Our analysis of crystal orientation under different processing conditions demonstrates that crystal orientation can be dictated by the thermal annealing temperature. This allows us to correlate photovoltaic device performance with crystal orientation. Figure 6 shows a plot of

average performance of P3HT9-*b*-PF8TBT as a function of annealing temperature. The melting transition for this material occurs around 230 °C. GIWAXS measurements also corroborate a change in P3HT crystal orientation in this temperature range. As can be readily seen, the effect of annealing above the melting transition, which produces a significant change in the P3HT crystal orientation, results in a lower photovoltaic power conversion efficiency. This is expected since charge mobility is known to be enhanced along the π stacking direction relative to the alkyl chain stacking direction,[33] and the crystal reorientation therefore should lead to reduced mobility between electrodes. However, only an effect of roughly 15-20 % is observed. This is much smaller than would be expected based on prior studies, and could potentially be due to degradation or other morphological changes at elevated temperatures. This result suggests that crystal orientation is not a predominant factor determining photovoltaic performance in the P3HT-*b*-PFTBT system and other factors, such as charge recombination, may be more dominant for dictating overall photovoltaic performance.

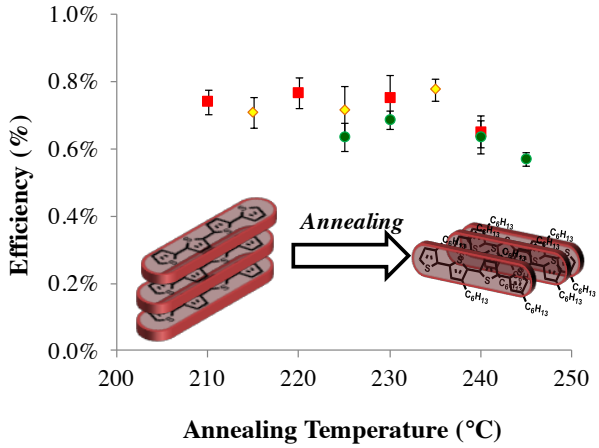

Figure 6: Comparison of photovoltaic device efficiency as a function of annealing temperature and P3HT crystal orientation for P3HT9-*b*-PF8TBT. The P3HT crystal orientation flips when annealed at or above 240 °C and cooled back to room temperature. Average efficiency and

standard deviations are plotted for three batches of devices (denoted with red squares, yellow triangles, and green circles) cast from similar conditions (8 mg ml^{-1} chloroform, 1500 rpm, ITO/PEDOT:PSS/Polymer/Al) annealed after aluminum deposition for 10 minutes at the specified temperature.

Next, we turn to polymer block segregation, also known as micro-phase segregation or block copolymer self-assembly. Our prior studies with P3HT-*b*-PFTBT revealed lamellar ordering with a characteristic domain size of 9 nm (*d*-spacing of 18 nm) and a preferential in-plane orientation under optimized processing conditions that produced near 3 % power conversion efficiencies.[15] To investigate block copolymer self-assembly in the systematic series of all-conjugated block copolymers, we analyzed films by grazing-incidence small-angle X-ray scattering (GISAXS) to assess domain sizes for films with various processing histories. GISAXS can reveal the presence of nanoscale domains that arise due to phase-segregation of the P3HT and PFTBT polymer blocks. Films were either thermally annealed at 165 °C or 230 °C or solvent annealed. These temperatures were chosen to be either above or below the crystal melting temperature of P3HT, roughly 220 °C. Solvent annealing was previously shown to give lamellar ordering in a related all-conjugated block copolymer.[38] Films were also cast from room-temperature or refluxing solvent, which we found in our previous study improved photovoltaic performance[3]. Small-angle X-ray scattering data is provided in Supporting Information Figure S9. For comparison, we analyzed selected homopolymer blends for evidence of large-scale phase separation. All blends studied showed clear evidence of phase separation between P3HT and PFTBT after annealing (see Supporting Information Figure S10).

Similar to what was observed in P3HT-*b*-PF8TBT,[15] most polymers used in this study exhibited a broad low-*q* peak characteristic of weak segregation, as shown in Figure 7 for P3HT-

b-PF6HTBT1. Measurement of the peak position in inverse space enables an estimate of the domain size produced through block segregation. However, we note that in many cases, no low-angle feature was observed and we were unable to estimate domain sizes from X-ray analysis. This suggests very weak or no block segregation for these samples, or insufficient annealing time. To extract the domain size from samples that exhibit a low-q peak (see Supporting Information Figure S9), we convert the q value at the peak position to an interdomain d-spacing using $d = 2\pi / q$. As detailed in Figure 3, the domain sizes that we measure for the present set of samples are roughly 6 – 10 nm, significantly smaller those observed in P3HT-*b*-PFTBT (18 nm)[15]. Since the individual domain sizes for each polymer block are approximately half of the domain spacing, this implies domain sizes on the order of 3-5 nm, significantly smaller than the expected exciton diffusion length.[39] The d-spacing is plotted as a function of molecular weight for all the samples analyzed, and the plot shows that the d-spacing is weakly dependent on molecular weight. We note that even in samples with higher molecular weights, the d-spacing is smaller when compared with P3HT-*b*-PF8TBT of a similar molecular weight. This suggests that the addition of side-chains decreases the driving force for block copolymer segregation, which may be due to the improved miscibility between P3HT and the PFTBT block when side-chains are added.

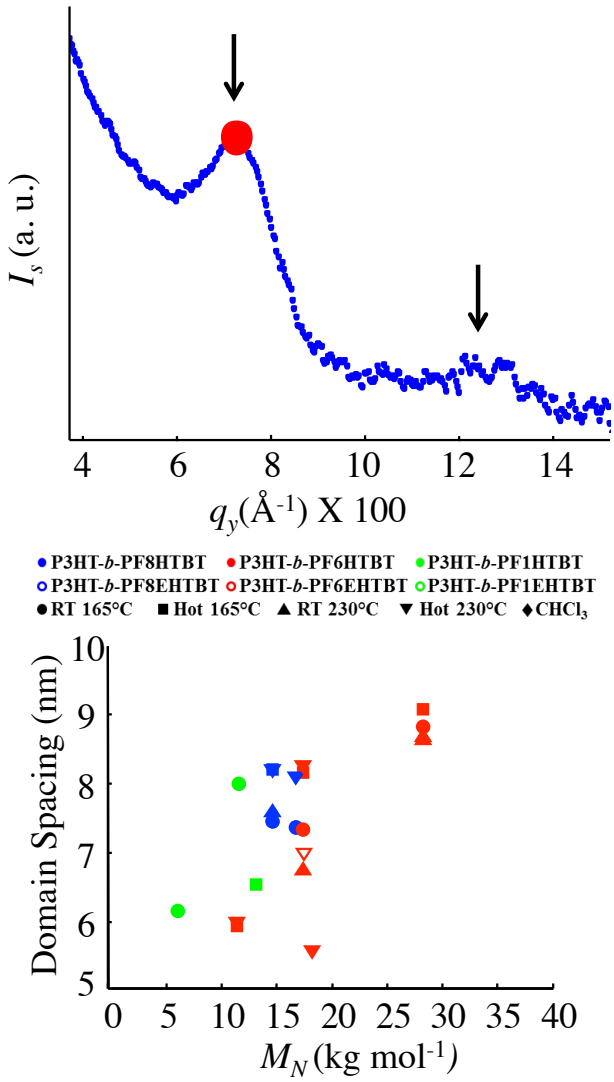

Figure 7: GISAXS analysis of conjugated block copolymer films. Representative example of scattered intensity P3HT-b-PF6HTBT1 (top) and domain-size measured by GISAXS as a function of number average molecular weight (M_N) and five different processing histories (bottom): the materials were spin cast from room temperature solvent and annealed at 165°C (●) or 230°C (▲) or spin-cast from from refluxing (Hot) solvent and annealed at 165°C (■) or 230°C (▼). Solvent annealing with room temperature chloroform (♦) was also tested. Alkyl chain lengths of 8, 6, and 1 on the fluorene unit of PFTBT are indicated by blue, red, and green

respectively. Side chains on the thiophene units of PFTBT are indicated by closed symbols (hexyl) and open symbols (ethyl-hexyl).

The small domain size is a concern since small domains may favor charge recombination in the film which would be detrimental to device performance.[32] Performance data of most block copolymer materials are shown in Figure 8, and full performance metrics including short-circuit current, open-circuit voltage, and fill factor are presented in the Supporting Information Table S3. For comparison, we have included in Table S3, three materials without side chains on the thiophene rings of the PFTBT block (P3HT-*b*-PF8TBT): the previously reported 3% materials[15] and two similar block copolymers of different molecular weight and P3HT content. As can be readily seen in Figure 2, the P3HT-*b*-PF8TBT materials uniformly outperform the materials with added side chains. Devices based on the P3HT-*b*-PF8TBT system have high short-circuit currents by at least an order of magnitude and higher open-circuit voltages and fill factors compared with devices based on block copolymers with added side-chains. This makes the poor performance of the materials with the additional side chains quite striking and indicates that the side chains are responsible for increased mixing or disrupt conjugation along the backbone, either of which could result in decreased performance.[32] Trends among our materials suggest that a balanced P3HT content (near 60%) and higher molecular weights yield improved performance, although these are weak trends in low-performance materials. Among the three P3HT-*b*-PF8TBT block copolymers studied, the highest performance was observed at a P3HT content of 56% (compared with 42% and 75%) and lower polydispersity (1.30 compared with 1.91 and 1.49).

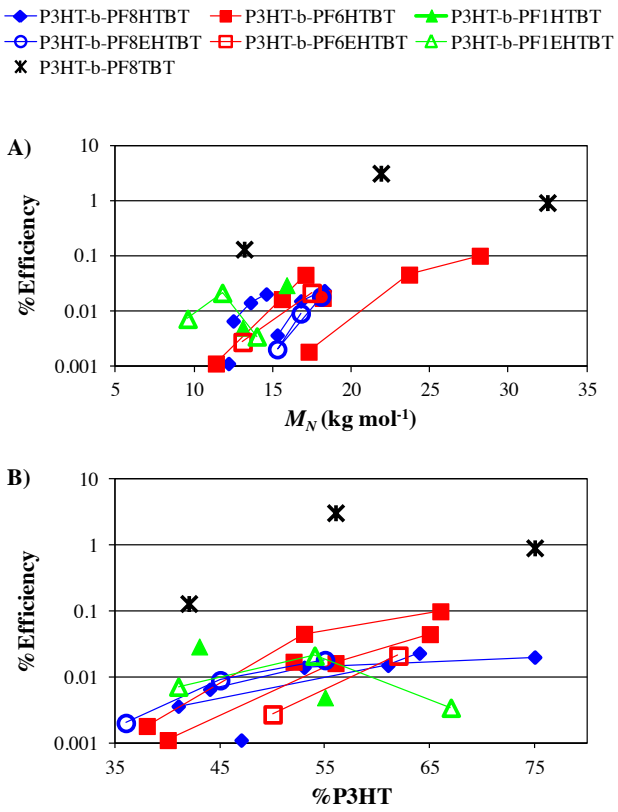

Figure 8: Plot of photovoltaic performance data as function of A) number average molecular weight M_N and B) P3HT content. Samples that have matcing P3HT blocks are connected with lines. The data is presented in tabular form in the Supporting Information Table S3. The maximum performance measured for optimized devices is plotted.

Conclusion

This study clearly indicates that the addition of side-chains, which has been found to enhance the performance of polymer blend photovoltaics, is detrimental to the performance of P3HT-*b*-PFTBT block copolymer systems. Morphological analysis reveals that crystalline orientation is independent of side-chain composition and primarily dependent on processing history. Further, we find that the crystal orientation has a relatively small impact (15-20 %) on power conversion

efficiency. GISAXS analysis reveals a significantly decreased *d*-spacing in our block copolymer samples with added side-chains relative to the P3HT-PF8TBT system which has no side-chain on the TBT unit. Hence, we conclude that small domain sizes and weak segregation are primarily responsible for the poor photovoltaic performance observed. This suggest that future work should focus on utilization of side-chains that increase the phase separation between polymer blocks, in contrast to strategies for improving polymer-blend solar cells which typically focus on increasing compatibility and reducing phase separation.[27,28]

Supporting Information. Experimental/instrumental details, characteristics of homopolymers and block copolymers, performance data in organic photovoltaic devices, ^{1}H NMR of block copolymers, film absorbance of PFTBT homopolymers, details on method to determine block copolymer purity, additional discussion on chi distribution analysis, plot of edge-on, face-on, and isotropic components as a function of annealing temperature, DSC data for polymers used in *in situ* measurements, temperature dependent GIWAXS measurements, GISAXS data for block copolymers, and *in situ* GIWAXS videos for P3HT2-*b*-PF8HTBT3 (P3HT2bPF8HTBT3_220C.mpg and P3HT2bPF8HTBT3_165C.mpg), P3HT9-*b*-PF8TBT (P3HT9bPF8TBT_165C.mpg), and P3HT7-*b*-PF8EHTBT1 (P3HT7bPF8EHTBT1_165C.mpg). This material is available free of charge via the Internet at http://pubs.acs.org.

Corresponding Author

Rafael Verduzco, rafaelv@rice.edu Rice University, 6100 Main St., MS 362, Houston, TX, USA, 77005

Author Contributions

The manuscript was written through contributions of all authors. All authors have given approval to the final version of the manuscript.

Funding Sources

This work was supported by the National Science Foundation CAREER program under Grant Nos. DMR-1352099, CBET-1264703, and CBET-1336073, the Shell Center for Sustainability, and Louis and Peaches Owen. Use of the Advanced Photon Source, an Office of Science User Facility operated for the U.S. Department of Energy (DOE) Office of Science by Argonne National Laboratory, was supported by the U.S. DOE under Contract No. DE-AC02-06CH11357. Use of the National Synchrotron Light Source and Center for Functional Nanomaterials, Brookhaven National Laboratory, were supported by the U.S. Department of Energy, Office of Science, Office of Basic Energy Sciences, under Contract No. DE-AC02-98CH10886. The work at Los Alamos National Laboratory (LANL) was supported by DoE Office of Basic Energy Sciences Work Proposal 08SPCE973 (W.N.and A.D.M.) and by the LANL LDRD program XW11 (A.D.M). This work was done in part at the Center for Integrated Nanotechnologies, an Office of Science User Facility.

REFERENCES

(1) Mazzio, K. A.; Luscombe, C. K. The Future of Organic Photovoltaics. *Chem. Soc. Rev.* **2014**, *44*, 78–90.
(2) Carlé, J. E.; Krebs, F. C. Technological Status of Organic Photovoltaics (OPV). *Sol. Energy Mater. Sol. Cells* **2013**, *119*, 309–310.
(3) Darling, S. B.; You, F.; Veselka, T.; Velosa, A. Assumptions and the Levelized Cost of Energy for Photovoltaics. *Energy Environ. Sci.* **2011**, *4*, 3133–3139.
(4) Gaudiana, R. Organic Photovoltaics: Challenges and Opportunities. *J. Polym. Sci. Part B Polym. Phys.*
(5) Huang, Y.; Kramer, E. J.; Heeger, A. J.; Bazan, G. C. Bulk Heterojunction Solar Cells: Morphology and Performance Relationships. *Chem. Rev.* **2014**, *114*, 7006–7043.
(6) Yassar, A.; Miozzo, L.; Gironda, R.; Horowitz, G. Rod–coil and All-Conjugated Block Copolymers for Photovoltaic Applications. *Prog. Polym. Sci.* **2013**, *38*, 791–844.

(7) Robb, M. J.; Ku, S.-Y.; Hawker, C. J. 25th Anniversary Article: No Assembly Required: Recent Advances in Fully Conjugated Block Copolymers. *Adv. Mater.* **2013**, *25*, 5686–5700.
(8) Topham, P. D.; Parnell, A. J.; Hiorns, R. C. Block Copolymer Strategies for Solar Cell Technology. *J. Polym. Sci. Part B Polym. Phys.* **2011**, *49*, 1131–1156.
(9) Botiz, I.; Darling, S. B. Optoelectronics Using Block Copolymers. *Mater. Today* **2010**, *13*, 42–51.
(10) Darling, S. B. Block Copolymers for Photovoltaics. *Energy Environ. Sci.* **2009**, *2*, 1266.
(11) Wang, J.; Ueda, M.; Higashihara, T. Synthesis and Morphology of All-Conjugated Donor–acceptor Block Copolymers Based on poly(3-Hexylthiophene) and Poly(naphthalene Diimide). *J. Polym. Sci. Part Polym. Chem.* **2014**, *52*, 1139–1148.
(12) Willot, P.; Moerman, D.; Leclère, P.; Lazzaroni, R.; Baeten, Y.; Van der Auweraer, M.; Koeckelberghs, G. One-Pot Synthesis and Characterization of All-Conjugated Poly(3-Alkylthiophene)-Block-poly(dialkylthieno[3,4-B]pyrazine). *Macromolecules* **2014**, *47*, 6671–6678.
(13) Yan, C.; Cadby, A. J.; Parnell, A. J.; Tang, W.; Skoda, M. W. A.; Mohamad, D.; King, S. P.; Reynolds, L. X.; Haque, S. A.; Wang, T.; *et al*. Photophysics and Morphology of a Polyfluorene Donor–acceptor Triblock Copolymer for Solar Cells. *J. Polym. Sci. Part B Polym. Phys.* **2013**, *51*, 1705–1718.
(14) Nakabayashi, K.; Mori, H. All-Polymer Solar Cells Based on Fully Conjugated Block Copolymers Composed of Poly(3-Hexylthiophene) and Poly(naphthalene Bisimide) Segments. *Macromolecules* **2012**, *45*, 9618–9625.
(15) Guo, C.; Lin, Y.-H.; Witman, M. D.; Smith, K. A.; Wang, C.; Hexemer, A.; Strzalka, J.; Gomez, E. D.; Verduzco, R. Conjugated Block Copolymer Photovoltaics with near 3% Efficiency through Microphase Separation. *Nano Lett.* **2013**, *13*, 2957–2963.
(16) McNeill, C. R.; Halls, J. J. M.; Wilson, R.; Whiting, G. L.; Berkebile, S.; Ramsey, M. G.; Friend, R. H.; Greenham, N. C. Efficient Polythiophene/Polyfluorene Copolymer Bulk Heterojunction Photovoltaic Devices: Device Physics and Annealing Effects. *Adv. Funct. Mater.* **2008**, *18*, 2309–2321.
(17) McNeill, C. R.; Abrusci, A.; Zaumseil, J.; Wilson, R.; McKiernan, M. J.; Burroughes, J. H.; Halls, J. J. M.; Greenham, N. C.; Friend, R. H. Dual Electron Donor/electron Acceptor Character of a Conjugated Polymer in Efficient Photovoltaic Diodes. *Appl. Phys. Lett.* **2007**, *90*, 193506–193506 – 3.
(18) Kang, H.; Uddin, M. A.; Lee, C.; Kim, K.-H.; Nguyen, T. L.; Lee, W.; Li, Y.; Wang, C.; Woo, H. Y.; Kim, B. J. Determining the Role of Polymer Molecular Weight for High-Performance All-Polymer Solar Cells: Its Effect on Polymer Aggregation and Phase Separation. *J. Am. Chem. Soc.* **2015**, *137*, 2359–2365.
(19) Zhou, Y.; Kurosawa, T.; Ma, W.; Guo, Y.; Fang, L.; Vandewal, K.; Diao, Y.; Wang, C.; Yan, Q.; Reinspach, J.; *et al*. High Performance All-Polymer Solar Cell via Polymer Side-Chain Engineering. *Adv. Mater.* **2014**, *26*, 3767–3772.
(20) Zhou, E.; Nakano, M.; Izawa, S.; Cong, J.; Osaka, I.; Takimiya, K.; Tajima, K. All-Polymer Solar Cell with High Near-Infrared Response Based on a Naphthodithiophene Diimide (NDTI) Copolymer. *ACS Macro Lett.* **2014**, *3*, 872–875.
(21) Mu, C.; Liu, P.; Ma, W.; Jiang, K.; Zhao, J.; Zhang, K.; Chen, Z.; Wei, Z.; Yi, Y.; Wang, J.; *et al*. High-Efficiency All-Polymer Solar Cells Based on a Pair of Crystalline Low-Bandgap Polymers. *Adv. Mater.* **2014**, *26*, 7224–7230.

(22) Mori, D.; Benten, H.; Okada, I.; Ohkita, H.; Ito, S. Low-Bandgap Donor/Acceptor Polymer Blend Solar Cells with Efficiency Exceeding 4%. *Adv. Energy Mater.* **2014**, *4*, 3.
(23) Earmme, T.; Hwang, Y.-J.; Subramaniyan, S.; Jenekhe, S. A. All-Polymer Bulk Heterojuction Solar Cells with 4.8% Efficiency Achieved by Solution Processing from a Co-Solvent. *Adv. Mater.* **2014**, *26*, 6080–6085.
(24) Mori, D.; Benten, H.; Ohkita, H.; Ito, S.; Miyake, K. Polymer/Polymer Blend Solar Cells Improved by Using High-Molecular-Weight Fluorene-Based Copolymer as Electron Acceptor. *ACS Appl. Mater. Interfaces* **2012**, *4*, 3325–3329.
(25) Schubert, M.; Dolfen, D.; Frisch, J.; Roland, S.; Steyrleuthner, R.; Stiller, B.; Chen, Z.; Scherf, U.; Koch, N.; Facchetti, A.; *et al*. Influence of Aggregation on the Performance of All-Polymer Solar Cells Containing Low-Bandgap Naphthalenediimide Copolymers. *Adv. Energy Mater.* **2012**, *2*, 369–380.
(26) Mulherin, R. C.; Jung, S.; Huettner, S.; Johnson, K.; Kohn, P.; Sommer, M.; Allard, S.; Scherf, U.; Greenham, N. C. Ternary Photovoltaic Blends Incorporating an All-Conjugated Donor–Acceptor Diblock Copolymer. *Nano Lett* **2011**, *11*, 4846–4851.
(27) Kang, H.; Kim, K.-H.; Choi, J.; Lee, C.; Kim, B. J. High-Performance All-Polymer Solar Cells Based on Face-On Stacked Polymer Blends with Low Interfacial Tension. *ACS Macro Lett.* **2014**, *3*, 1009–1014.
(28) Hwang, Y.-J.; Earmme, T.; Courtright, B. A. E.; Eberle, F. N.; Jenekhe, S. A. N-Type Semiconducting Naphthalene Diimide-Perylene Diimide Copolymers: Controlling Crystallinity, Blend Morphology, and Compatibility Toward High-Performance All-Polymer Solar Cells. *J. Am. Chem. Soc.* **2015**, *137*, 4424–4434.
(29) Sommer, M.; Komber, H.; Huettner, S.; Mulherin, R.; Kohn, P.; Greenham, N. C.; Huck, W. T. S. Synthesis, Purification, and Characterization of Well-Defined All-Conjugated Diblock Copolymers PF8TBT-B-P3HT. *Macromolecules* **2012**, *45*, 4142–4151.
(30) Lin, Y.-H.; Smith, K. A.; Kempf, C. N.; Verduzco, R. Synthesis and Crystallinity of All-Conjugated poly(3-Hexylthiophene) Block Copolymers. *Polym. Chem.* **2013**, *4*, 229.
(31) Verduzco, R.; Botiz, I.; Pickel, D. L.; Kilbey, S. M.; Hong, K.; Dimasi, E.; Darling, S. B. Polythiophene-Block-Polyfluorene and Polythiophene-Block-Poly(fluorene-Co-Benzothiadiazole): Insights into the Self-Assembly of All-Conjugated Block Copolymers. *Macromolecules* **2011**, *44*, 530–539.
(32) Sommer, M.; Komber, H.; Huettner, S.; Mulherin, R.; Kohn, P.; Greenham, N. C.; Huck, W. T. S. Synthesis, Purification, and Characterization of Well-Defined All-Conjugated Diblock Copolymers PF8TBT-B-P3HT. *Macromolecules* **2012**, *45*, 4142–4151.
(33) Sirringhaus, H.; Brown, P. J.; Friend, R. H.; Nielsen, M. M.; Bechgaard, K.; Langeveld-Voss, B. M. W.; Spiering, A. J. H.; Janssen, R. a. J.; Meijer, E. W.; Herwig, P.; *et al*. Two-Dimensional Charge Transport in Self-Organized, High-Mobility Conjugated Polymers. *Nature* **1999**, *401*, 685–688.
(34) Osaka, I.; McCullough, R. D. Advances in Molecular Design and Synthesis of Regioregular Polythiophenes. *Acc Chem Res* **2008**, *41*, 1202–1214.
(35) Hlaing, H.; Lu, X.; Hofmann, T.; Yager, K. G.; Black, C. T.; Ocko, B. M. Nanoimprint-Induced Molecular Orientation in Semiconducting Polymer Nanostructures. *ACS Nano* **2011**, *5*, 7532–7538.
(36) Johnston, D. E.; Yager, K. G.; Hlaing, H.; Lu, X.; Ocko, B. M.; Black, C. T. Nanostructured Surfaces Frustrate Polymer Semiconductor Molecular Orientation. *ACS Nano* **2014**, *8*, 243–249.

(37) Sepe, A.; Rong, Z.; Sommer, M.; Vaynzof, Y.; Sheng, X.; Müller-Buschbaum, P.; Smilgies, D.-M.; Tan, Z.-K.; Yang, L.; Friend, R. H.; *et al*. Structure Formation in P3HT/F8TBT Blends. *Energy Environ. Sci.* **2014**, *7*, 1725–1736.
(38) Lin, Y.-H.; Yager, K. G.; Stewart, B.; Verduzco, R. Lamellar and Liquid Crystal Ordering in Solvent-Annealed All-Conjugated Block Copolymers. *Soft Matter* **2014**, *10*, 3817–3825.
(39) Haugeneder, A.; Neges, M.; Kallinger, C.; Spirkl, W.; Lemmer, U.; Feldmann, J.; Scherf, U.; Harth, E.; Gügel, A.; Müllen, K. Exciton Diffusion and Dissociation in Conjugated Polymer/fullerene Blends and Heterostructures. *Phys. Rev. B* **1999**, *59*, 15346–15351.

Insert Table of Contents Graphic and Synopsis Here

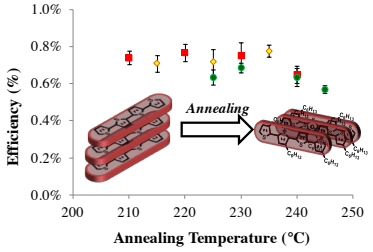

A library of 30 donor-block-acceptor all-conjugated block copolymers is prepared and studied to investigate the effect of side-chains and processing conditions on crystal orientation and photovoltaic device performance. The orientation of P3HT crystallites is robust to various alkyl side chains on the PFTBT and is dependent only on annealing temperature, with edge-on and face-on orientations observed for annealing temperatures above and below the P3HT melting transition, respectively. We find that crystal orientation has only a modest effect on performance while the addition of side-chains is detrimental to performance for a wide range of side-chain types and polymer molecular weights. This work suggests that future work aimed at improving

block copolymer OPV device should focus on increasing domain sizes and segregation strength between polymer blocks